ESTIMATION PROCEDURE OF ELASTIC-PLASTIC *J* FRACTURE PARAMETER FOR CIRCUMFERENTIAL CRACKED PIPES SUBJECTED TO BENDING MOMENT

Mario Sérgio Giancoli Chiodo, mario.sg@gmail.com
Luís Fernando Schiano Parise, luis.parise@gmail.com
Claudio Ruggieri, claudio.ruggieri@usp.br
Department of Naval Architecture and Ocean Engineering, PNV-EPUSP
University of São Paulo, São Paulo, SP 05508−900, Brazil

Abstract *– This work provides an estimation procedure to determine the J-integral for pipes with circumferential surface cracks subjected to bending load for a wide range of crack geometries and material (hardening) based upon fully-plastic solutions. A summary of the methodology upon which J is derived sets the necessary framework to determine nondimensional functions h_1 applicable to a wide range of crack geometries and material properties characteristic of structural, pressure vessel and pipeline steels. The extensive nonlinear, 3-D numerical analyses provide a definite full set of solutions for J which enters directly into fitness-for-service (FFS) analyses and defect assessment procedures of cracked pipes and cylinders subjected to bending load.*

Keywords*: J-integral, fully plastic solutions, circumferential surface crack, pipeline*

1. INTRODUCTION

Defect assessment procedures of cracked pipes and cylinders under varying loading conditions rely heavily on the accurate evaluation of crack driving forces, such as the (Mode I) linear elastic stress intensity factor, K_I, and the elastic-plastic *J*-integral (or, equivalently, the crack tip opening displacement, CTOD or δ). These measures of crack-tip loading provide a means to correlate the severity of crack-like defects to the operating conditions in terms of the simple axiom that fracture occurs when the applied crack driving force reaches a critical value as given by K_{Ic}, J_c or δ_c [1-3]. Previous research efforts have provided an extensive body of K_I solutions for a variety of crack configurations, including circumferentially cracked cylinders, which are readily available through several compendia [4-8]. In contrast, a full set of *J* and CTOD solutions for varying crack geometries and loading modes directly connected to the description of fracture behavior under large scale yielding conditions is still lacking.

Current evaluation procedures for *J* focus primarily on developing estimation schemes for its plastic component, denoted J_p. These methodologies have evolved essentially along three lines of development: (1) estimation procedures relating the plastic contribution to the strain energy and *J*; (2) fully plastic descriptions of *J* based upon HRR-controlled crack-tip fields and limit load solutions and (3) approximate descriptions of *J* derived from the concept of a reference stress coupled with stress intensity factor solutions. The first approach employs a plastic η-factor introduced by Sumpter and Turner [9] to relate the macroscale crack driving force (*J* and CTOD) to the area under the load versus load line displacement (or crack mouth opening displacement) for cracked configurations (see also refs. [10,11]). Because of its relative ease with which the load-displacement records can be measured in conventional test specimens, the method is most suited for testing protocols to measure fracture toughness such as ASTM E1820 [12]. The second approach derives from previous work of Kumar et al. [13] building upon early investigation of Shih and Hutchinson [14] to introduce an estimation procedure for J_p applicable to elastic-plastic materials following a power hardening law such as the Ramberg-Osgood model [2,7,15]. Here, J_p is expressed in the general form $J_p \propto h_1(a/W, \mathcal{L}, n)(\mathcal{P}/\mathcal{P}_0)^{n+1}$ where a is the crack size, W denotes the component width, $\mathcal{L}$ represents a characteristic length for the cracked component, n is the Ramberg-Osgood strain hardening exponent, $\mathcal{P}$ defines a generalized load and $\mathcal{P}_0$ is the corresponding (plastic) limit load. Factor h_1 represents a nondimensional parameter dependent upon crack size, component geometry and strain hardening properties which simply scales J_p with $(\mathcal{P}/\mathcal{P}_0)^{n+1}$. The method became widely known as the EPRI methodology and has later been expanded

by Zahoor [16] to include additional geometries such as circumferentially and axially cracked pipes under tensile and bending loads. However, these *J* solutions for circumferentially cracked pipes subjected to bending remain limited to very few crack geometries and strain hardening properties. The third approach, most often referred to as the reference stress approach, is essentially a modification of the EPRI methodology proposed by Ainsworth [17] to reflect more closely the flow behavior of actual materials, particularly high hardening materials such as austenitic stainless steels. Moreover, this approach enables evaluation of J_p from simply using available stress intensity factor solutions for the cracked component in connection with the adoption of parameter h_1 defined for a linear material in which $n = 1$.

While all these procedures share much in common, each method has certain relative advantages and disadvantages in fracture mechanics applications. In particular, both the fully plastic (EPRI) and the reference stress methods prove sufficiently applicable for a broad range of crack geometries and loading modes. Further, they provide essentially similar estimates of crack driving forces for low to moderate deformation levels, as measured by *J* (CTOD), when the material's stress-strain behavior is adequately described by a power hardening law such as the Ramberg-Osgood model. However, this picture becomes potentially more complex as the evolving plasticity progresses from contained to fully yielded conditions, particularly for moderate to low hardening materials. Because parameter h_1 depends rather strongly on the strain hardening exponent (this issue is addressed later in Section 4), adopting h_1 for a linear material with $n = 1$ in Ainsworth's model can lead to unacceptably large errors in *J* estimations, especially for moderate to large *n*-values. While previous exploratory analyses by Anderson [2] have shown that both approaches provide similar predictions of critical crack sizes in center cracked panels, extension of these methodologies in accurate descriptions of crack-tip driving forces (as measured by *J* and CTOD) for circumferentially cracked pipes under conditions of varying cracking geometries, material properties and loading modes remains untested. These observations clearly underlie the need of reliable and yet simple evaluation procedures for crack-tip driving forces in advanced defect assessment methodologies applicable to elastic-plastic and fully plastic conditions.

The extension of fully plastic solutions for the *J*-integral in pipes with circumferential surface cracks subjected to bending load for a wide range of crack geometries and strain hardening properties is the focus of this paper. The present investigation broadens the applicability of current evaluation procedures for *J* which enter directly into structural integrity analyses and flaw tolerance criteria. The presentation begins with a summary of the fully-plastic solution upon which *J* is derived which forms the basis of the adopted framework to determine the elastic-plastic crack-tip driving forces for the analyzed cracked configurations. This is followed by the description of extensive 3-D nonlinear analyses of circumferentially cracked pipe with surface flaws having different crack depth (a) over pipe wall thickness (t) ratios and varying crack length for different strain hardening properties. The 3-D results cover a large set of dimensionless functions relating the elastic-plastic crack-tip driving forces with the applied (remote) bending moment applicable to FFS procedures of a wide range of thin-walled cylindrical components.

2. FULLY PLASTIC SOLUTIONS FOR THE *J*-INTEGRAL IN CIRCUMFERENTIALLY CRACKED PIPES

The procedure to estimate the *J* Integral for a cracked component such as a circumferentially cracked pipe begins by considering the elastic and plastic contributions to the strain energy under Mode I deformation in the form [2]

$$J = J_e + J_p \tag{1}$$

where the elastic component, J_e, is given by

$$J_e = \frac{K_I^2}{E'} \quad . \tag{2}$$

Here, K_I is where the elastic stress intensity factor and $E' = E$ or $E' = E/(1-\nu^2)$ whether plane stress or plane strain conditions are assumed with E representing the (longitudinal) elastic modulus and ν is the Poisson's ratio.

The plastic component, J_p, can be conveniently evaluated from the fully plastic solution for a strain hardening material introduced by Shih and Hutchinson [14] and further validated by Kumar et al. [13]. For an elastic–plastic material obeying a Ramberg-Osgood model [2,7,15] to describe the uniaxial true stress ($\bar{\sigma}$) vs. logarithmic strain ($\bar{\epsilon}$) response given by

$$\frac{\bar{\epsilon}}{\epsilon_{ys}} = \frac{\bar{\sigma}}{\sigma_{ys}} + \alpha\left(\frac{\bar{\sigma}}{\sigma_{ys}}\right)^n \tag{3}$$

where α is a dimensionless constant, n defines the strain hardening exponent, and σ_{ys} and $\epsilon_{ys} = \sigma_{ys}/E$ define the yield stress and strain , the fully plastic J_p is expressed as

$$J_p = \alpha \epsilon_{ys} \sigma_{ys} b h_1(a/W, \mathcal{L}, n) \left(\frac{\mathcal{P}}{\mathcal{P}_0} \right)^{n+1} \tag{4}$$

where a is the crack size, W denotes the cracked component width, $b = W - a$ defines the uncracked ligament, $\mathcal{L}$ represents a characteristic length for the cracked component, $\mathcal{P}$ is a generalized load and $\mathcal{P}_0$ is the corresponding (generalized) limit load. In the above expression, h_1 is a dimensionless factor dependent upon crack size, component geometry and strain hardening properties. The previous solution forJ_p is essentially applicable for fully plastic cracked configurations in which the elastic strains are vanishingly small, particularly within the annular region surrounding the crack tip where the condition $J \propto \mathcal{P}^{n+1}$ holds true [18].

To introduce an estimation procedure for J in a cylinder or pipe having a circumferential surface crack based upon the previous fully-plastic solution, consider the crack configuration subjected to bend loading illustrated in Fig. 1. The above methodology can be extended in straightforward manner to define J_p for this crack geometry by the following expression

$$J_p = \alpha \epsilon_{ys} \sigma_{ys} b h_1(a/t, D_e/t, \theta, n) \left(\frac{M}{M_0} \right)^{n+1} \tag{5}$$

where D_e is the pipe (cylinder) outer diameter, t is the wall thickness, M denotes the applied bending moment and M_0 defines the limit bending moment. Here, the uncracked ligament is now given by $b = t - a$ and the surface crack length is described by the angle θ (see Fig. 1) as [7,16]

$$\theta = \frac{\pi c}{2 D_e} \tag{6}$$

where c is the circumferential crack half-length.

In the above expressions, the limit bending moment, M_0, is conventionally given by [7,16]

$$M_0 = 2 \sigma_{ys} R_m^2 t \left(2 \sin\beta - \frac{a}{t} \sin\theta \right) \tag{7}$$

in which R_m denotes the mean radius ($R_m = (R_e + R_i)/2$ where R_e and R_i are the external and internal radius) and parameter β is defined as

$$\beta = \frac{\pi}{2} \left[1 - \left(\frac{\theta}{\pi} \right) \left(\frac{a}{t} \right) \right] \quad . \tag{8}$$

The limit solution for the bending moment given by Eq. (7) is applicable in the range $(\theta + \beta) \leq \pi$ [16,7].

Finally, the elastic terms J_e, is calculated by using Eqs. (2) coupled with a convenient form for the elastic stress intensity factor, K_{I}. For a circumferential surface crack in a pipe subjected to a bending moment, an improved expression for parameter K_{I} is given by [7]

$$K_{\mathrm{I}} = \sigma_b G_5 \sqrt{\frac{\pi a}{Q_s}} \tag{9}$$

where σ_b is the (global or net-section) bending stress about the X-axis (see Fig. 1) expressed as

$$\sigma_b = \frac{4 M R_e}{\pi \left(R_e^4 - R_i^4 \right)} \tag{10}$$

and the flaw shape parameter, Q_s, is defined as

$$Q_s = 1 + 1.464 \left(\frac{a}{c} \right)^{1.65} \quad , \quad a \leq c \quad . \tag{11}$$

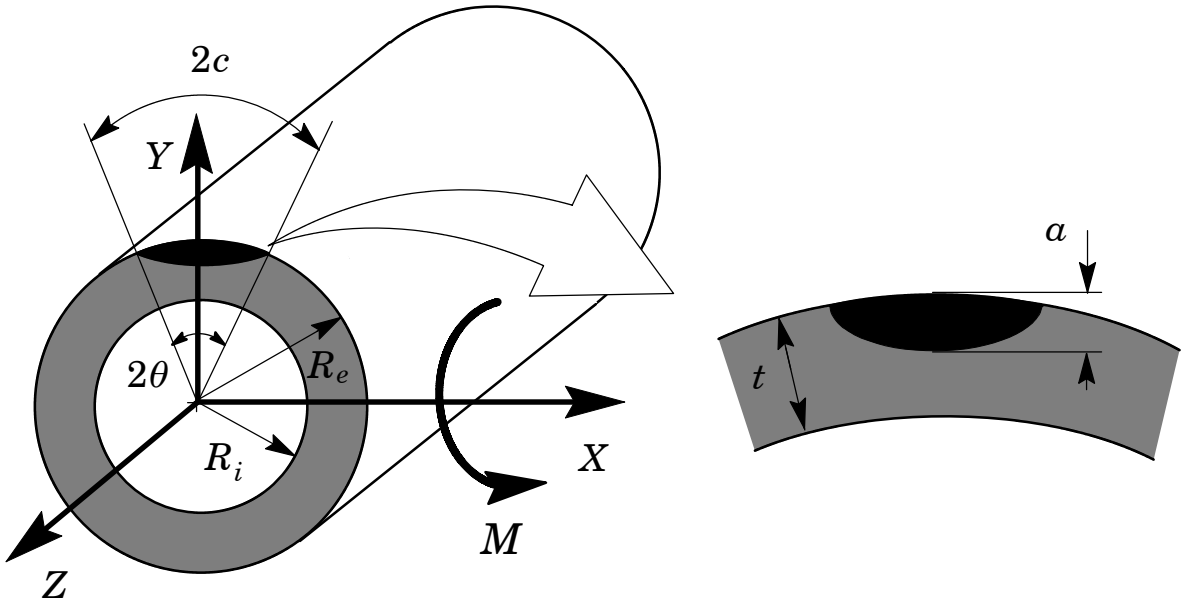

Figure 1 *Pipe configuration and defect geometry adopted in the numerical analyses.*

In the above expression (9), G_5 is the influence coefficient corresponding to a circumferential semi-elliptical surface crack in a cylinder subjected to a (pure) net-section bending as given in Appendix C of API 579 [7].

Evaluation of parameters J based upon the procedure outlined above requires specification of factors h_1 once all other quantities entering directly into the calculation of J_e and J_p are defined. Current available solutions (such as the EPRI methodology [13,18]) provide values for factor h_1 which are only applicable to few selected crack geometries, including circumferentially cracked pipes under axial load. The relatively limited analyses and data available to evaluate J for a broad range of crack geometries and material properties underscore the need for improved and accurate descriptions of factors h_1 for circumferential surface cracks in pipes under bending. Section 4 explores detailed numerical and validation analyses which lead to a comprehensive body of fully-plastic solutions for the J-integral.

3. Computational Procedures and Finite Element Models

3.1 Numerical Models of Circumferentially Cracked Pipes

Nonlinear 3-D finite element analyses are conducted on circumferentially cracked pipes with external surface flaws subjected to bending. The analyzed pipe models have wall thickness $t =$ 20.6 mm with different outside diameters $D_e = 206$ mm ($D_e/t = 10$), $D_e = 309$ mm ($D_e/t = 15$) and $D_e = 412$ mm ($D_e/t = 20$). These geometries typify current trends in high pressure, high strength pipelines, including submarine pipelines and risers. The analysis matrix considers surface flaws with varying crack depth (a) and crack length ($2c$) as defined by $a/t = 0.1$ to 0.5 with increments of 0.05 and $\theta/\pi = 0.04$, 0.08, 0.12, 0.16 and 0.20 ($1.7 \le c/a \le 82.5$ – see Eq. (6)). Figure 1 shows the pipe configuration and defect geometry adopted in the analyses. Overall, the computations comprised 135 numerical models and 405 loading cases considering the three hardening levels adopted in the analyses (refer to Section 3.2 next).

Figure 2(a-b) shows the finite element model constructed for the pipe with $D_e/t = 10$, $a/t = 0.5$ and $\theta/\pi = 0.12$. A conventional mesh configuration having a focused ring of elements surrounding the crack front is used with a small key-hole geometry (blunt tip) at the crack tip to enhance numerical convergence and to accommodate the large plastic strains that develop with increased levels of deformation. The small initial root radius at the crack tip is $\varrho_0 = 5\mu$m (0.005 mm). A typical half-symmetric model for the cracked pipes has approximately 15000 elements and 18000 nodes with appropriate constraints imposed on nodes defining the symmetry planes. The crack front is described by 15 (circumferential) layers defined over the crack half-length (c); the thickest layer is defined at the deepest point of the crack with thinner layers defined near the free surface to accommodate the strong gradient in the stress distribution along the crack front. The finite

element models for the pipe specimens are loaded by a four-point bending scheme so that a constant bending moment with zero shear forces is imposed on the crack plane and along the pipe length at distances about three times the pipe diameter. Very similar finite element models and mesh details are employed for other cracked pipe configurations.

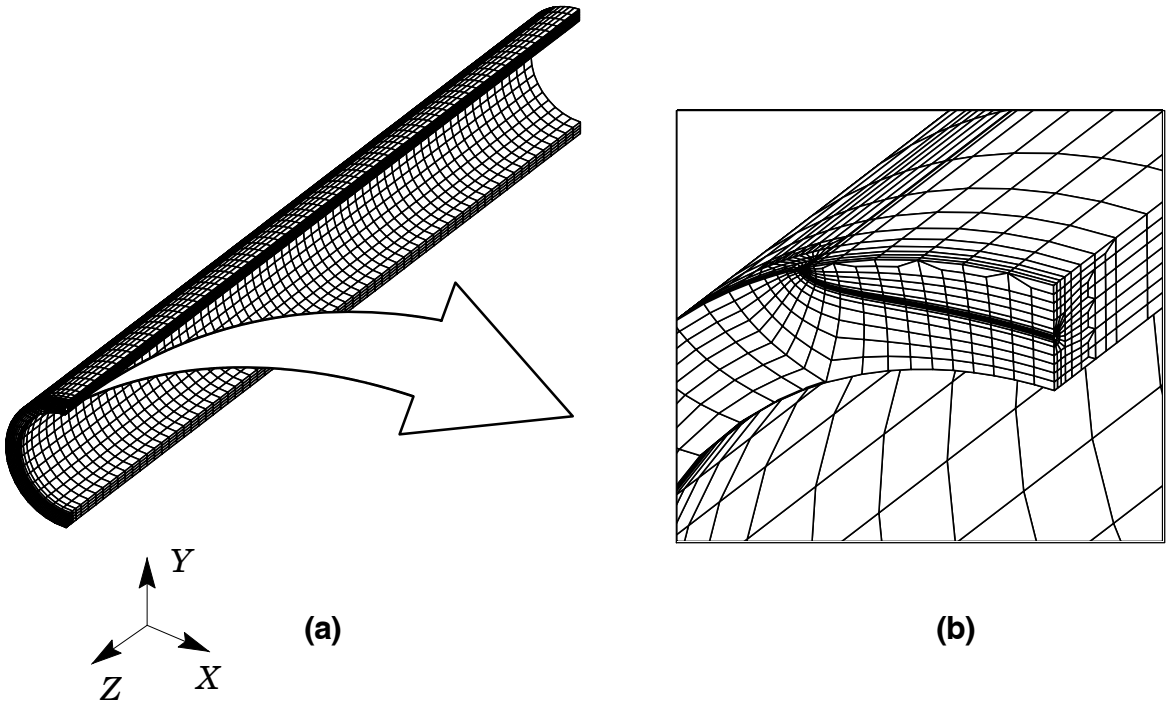

Figure 2 *(a) 3-D finite element model employed for the pipe specimen with $D_e/t = 10$, $a/t = 0.5$ and $\theta/\pi = 0.12$; (b) Near-tip model and meshing details.*

3.2 Material Models and Computational Procedures

The elastic-plastic constitutive model employed in all analyses reported here follows a J_2 flow theory with conventional Mises plasticity in small geometry change (SGC) setting. The numerical solutions employ a simple power-hardening model to characterize the uniaxial true stress ($\bar{\sigma}$) *vs.* logarithmic strain ($\bar{\epsilon}$) in the form

$$\frac{\bar{\epsilon}}{\epsilon_{ys}} = \frac{\bar{\sigma}}{\sigma_{ys}} \quad \bar{\epsilon} \le \epsilon_{ys} \;\; ; \qquad \frac{\bar{\epsilon}}{\epsilon_{ys}} = \alpha \left(\frac{\bar{\sigma}}{\sigma_{ys}} \right)^n \quad \bar{\epsilon} > \epsilon_{ys} \tag{12}$$

where σ_{ys} and ϵ_{ys} are the (yield) stress and strain, α is a dimensionless constant and n is the strain hardening exponent. The finite element analyses consider material flow properties covering typical structural, pressure vessel and pipeline grade steels with $E = 206$ GPa, $\nu = 0.3$ and $\alpha = 1$: $n = 5$ and $E/\sigma_{ys} = 800$ (high hardening material), $n = 10$ and $E/\sigma_{ys} = 500$ (moderate hardening material), $n = 20$ and $E/\sigma_{ys} = 300$ (low hardening material). These ranges of properties also reflect the upward trend in yield stress with the increase in strain hardening exponent, n, characteristic of ferritic structural steels, including pipeline steels.

3.3 Computational Procedures

The finite element code WARP3D [19] provides the numerical solutions for the 3-D analyses reported here. The code incorporates a Mises (J_2) constitutive model in both small-strain and finite-strain framework and solves the equilibrium equations at each iteration using a very efficient, sparse matrix solver highly tuned for Unix and PC based architectures. Use of the so-called $\overline{\boldsymbol{B}}$ formulation [20] precludes mesh lock-ups that arise as the deformation progresses into fully plastic, incompressible modes. The sparse solver significantly reduces both memory and CPU time required for solution of the

linearized equations compared to conventional direct solvers. A domain integral procedure [21] is utilized to compute the numerical values of J needed to determine the dimensionless function h_1. These J-values are in excellent agreement with estimation schemes based upon *eta*-factors for deformation plasticity [12] in common fracture specimens while, at the same time, retaining strong path independence for domains defined outside the highly strained material near the crack tip.

4. FACTORS h_1 FOR CIRCUMFERENTIAL SURFACE CRACKS IN PIPES UNDER BENDING

Evaluation of factor h_1 for the analyzed crack configurations follows from solving Eqs. (5) upon computation of the plastic component of the J integral, J_p, with the applied bending moment, M, for a given crack size, component geometry and strain hardening exponent, n. To develop a more consistent scheme to determine the dimensionless function h_1, it proves convenient to rewrite Eq. (5) into the form

$$\bar{J}_p = \frac{J_p}{\alpha \epsilon_{ys} \sigma_{ys} b} = h_1(a/t, D_e/t, \theta, n)\left(\frac{M}{M_0}\right)^{n+1} \tag{13}$$

so that factor h_1 can be obtained by simply determining the slope of a least square fit to the (linear) evolution of $\bar{J}_p$ with $(M/M_0)^{n+1}$.

Figures 3-5 provide the h_1-factors for the circumferentially cracked pipes with varying geometries and material properties derived from the J estimation procedure previously outlined. For all sets of analyses, the results reveal that factor h_1 displays a rather strong sensitivity to crack geometry and strain hardening behavior. To facilitate interpretation of these results, direct first attention to a fixed D_e/t-ratio such as the plots for $D_e/t = 10$ displayed in Fig. 3. For shallow crack sizes ($a/t < 0.2 \sim 0.3$), the h_1-values are fairly insensitive to crack length (defined by parameter θ/π) for all hardening levels; here, the evolution of factor h_1 with crack depth essentially falls onto a single curve particularly for $a/t < 0.2$. In contrast, the h_1-factors for deeply cracked pipes ($a/t > 0.4$) depend rather strongly on θ/π for all hardening levels, particularly for shorter crack lengths ($\theta/\pi \le 0.12$). Very similar trends are displayed by other D_e/t-ratios – see Figs. 4 and 5.

Further, we note that the evolution of factor h_1 with θ/π for a fixed a/t-ratio displays a somewhat mixed behavior as it increases and then slightly decreases with increased θ/π-values. Such development is particularly prominent in the deep crack range ($a/t > 0.4$) for all hardening levels. Consider, for example, the h_1-values for $n = 10$ and $a/t = 0.5$ displayed in Fig. 3(b); here, factor h_1 changes rapidly from $\theta/\pi = 0.04$ to $\theta/\pi = 0.08$ and then exhibits a slight drop from the peak level attained at $\theta/\pi = 0.12$ with increased crack length. We argue that these trends in variation of factor h_1 are associated with the synergistic combination of crack depth (which defines the crack ligament size) and circumferential crack length. Such synergism potentially impacts the evolution of the highly-strained plastic zones along the crack ligament with increased crack-tip loading thereby affecting the proportional relationship between $\bar{J}_p$ and. $(M/M_0)^{n+1}$ upon which h_1 is defined.

The results for the h_1-values corresponding to the low hardening material ($n = 20$) shown in the plots of Figs. 3-5 also deserve attention. As we have previously discussed, factor h_1 is evaluated using a range of J-values in which they follow a proportional relationship with the applied bending moment, M. While this condition is met for the full range of a/t-values and $\theta/\pi = 0.04$, 0.08 for all D_e/t-ratios, the h_1 evaluation procedure for some combinations of crack depth (a/t) and crack length (θ/π) for the $n = 20$ material fails to provide sufficiently accurate values. For a/t-ratios up through ~ 0.25, however, a full set of h_1-factors for the low hardening material and varying D_e/t-ratios is readily defined.

5. SUMMARY AND CONCLUSIONS

This work provides an estimation procedure to determine the J-integral for pipes with circumferential surface cracks subjected to bending load for a wide range of crack geometries and material properties based upon fully plastic solutions. In the present study, attention is directed to a circumferentially cracked pipe with surface flaws having different crack depth (a) over pipe wall thickness (t) ratios and varying crack length for different strain hardening properties and outside diameters (D_e/t). The methodology derives from a fully plastic description of the J-integral incorporating limit load solutions for the cracked component to determine nondimensional functions h_1 applicable to a wide range of crack geometries and material properties characteristic of structural, pressure vessel and pipeline steels.

The extensive set of nonlinear, 3-D finite element analyses conducted in this study provides a definite full set of solutions for J which enters directly into fitness-for-service (FFS) analyses and defect assessment procedures of cracked pipes and cylinders subjected to bending load. The associated dimensionless h-values are derived from a least square fitting to the linear evolution of normalized J_p with $(M/M_0)^{n+1}$ for quantities which follow a proportional dependence of J_p

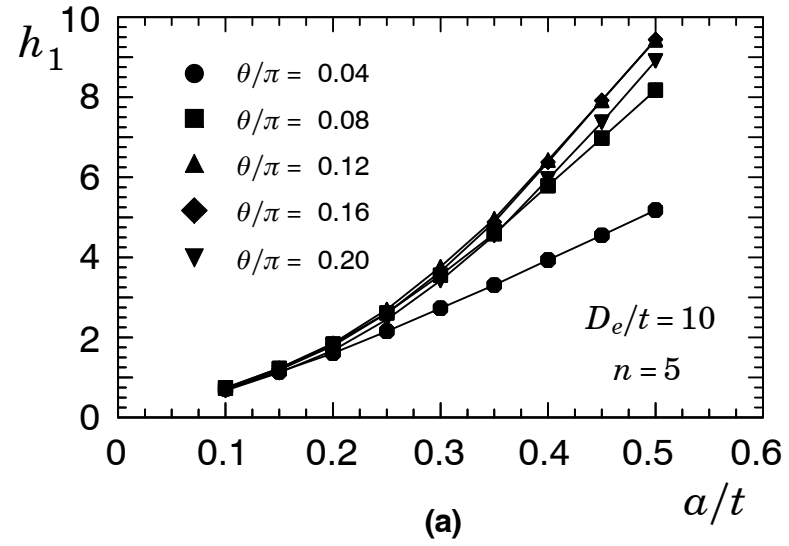

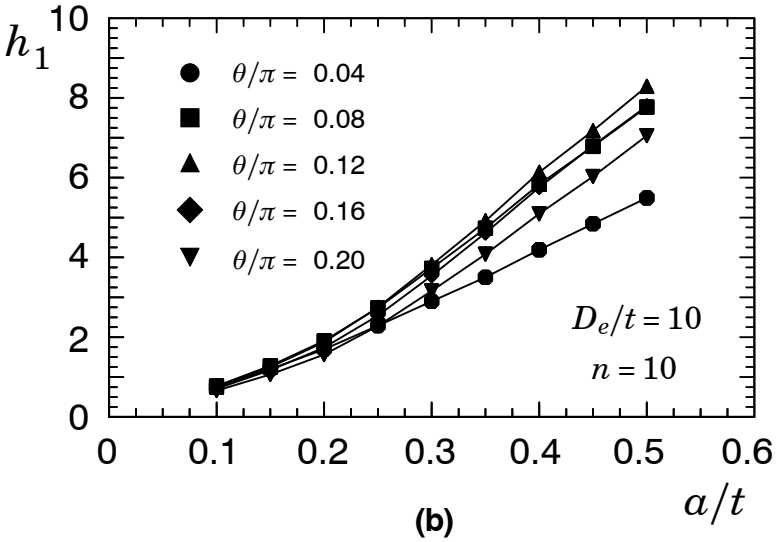

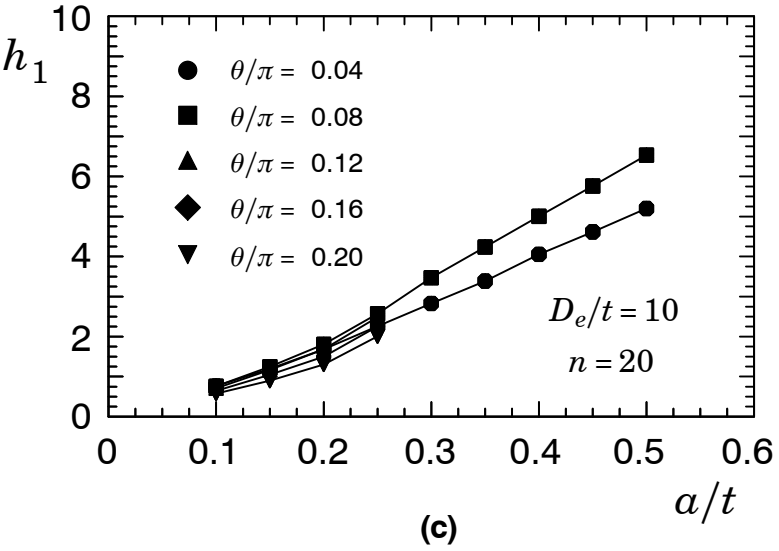

Figure 3 *Variation of factor h_1 with increased a/t-ratio for the pipe specimen with $D_e/t = 10$.*

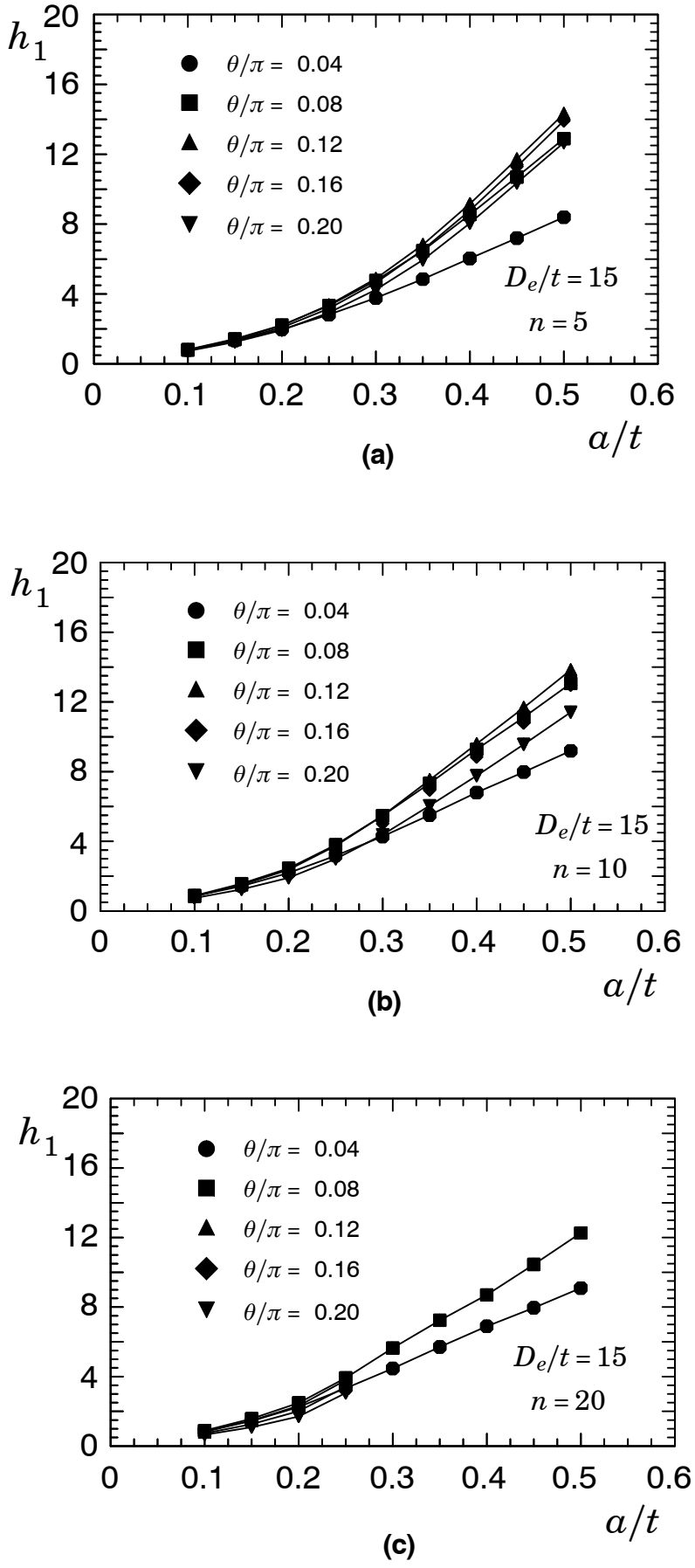

Figure 4 *Variation of factor h_1 with increased a/t-ratio for the pipe specimen with $D_e/t = 15$.*

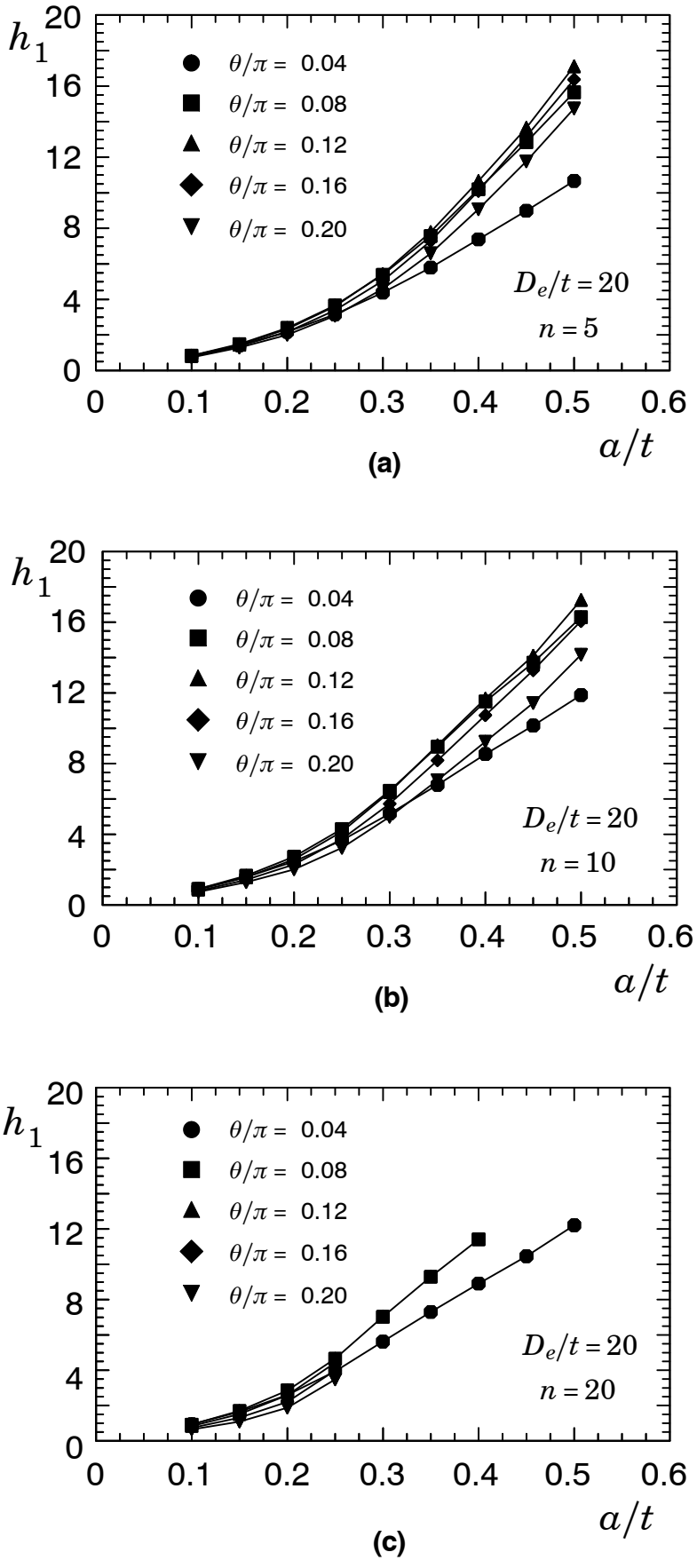

Figure 5 *Variation of factor h_1 with increased a/t-ratio for the pipe specimen with $D_e/t = 20$.*

on the applied loading (M). Ongoing work with the fully plastic solution framework also focuses on deriving h-values for circumferentially cracked pipes under combined bending, tension and internal pressure as well as for overmatched girth welds.

6. ACKNOWLEDGMENTS

This investigation was supported by the Brazilian State Oil Company (Petrobras). The work of C. Ruggieri and M. S. G. Chiodo was also supported by the Brazilian Council for Scientific and Technological Development (CNPq). The authors are indebted to Eduardo Hippert Jr. and Guilherme V. P. Donato (CENPES−Petrobras) for his valuable contributions and useful discussions.

7. REFERENCES

[1] Hutchinson, J. W., ''Fundamentals of the Phenomenological Theory of Nonlinear Fracture Mechanics,'' *Journal of Applied Mechanics*, Vol. 50, pp. 1042-1051, 1983.
[2] Anderson, T. L., *Fracture Mechanics: Fundaments and Applications*, 3rd Edition, CRC Press, Boca Raton, 2005.
[3] Saxena, A., *Nonlinear Fracture Mechanics for Engineers*, CRC Press, Boca Raton, 1998.
[4] Tada, H., Paris, P. C. and Irwin, G. R., *The Stress Analysis of Cracks Handbook*, 2nd Editions, Paris Productions, St. Louis, 1985.
[5] British Standard Institution. "Guide on Methods for Assessing the Acceptability of Flaws in Metallic Structures," BS7910, 2005.
[6] SINTAP: Structural Integrity Assessment Procedure for European Industry. Final Procedure, 1999.
[7] American Petroleum Institute. "Fitness-for-Service", API RP-579-1 / ASME FFS-1, 2007.
[8] Marie, S., Chapuliot, S., Kayser, Y., Lacire, M. H., Drubay, B., Barthelet, B., Le Delliou, P., Rougie, V., Naudin, C., Gilles, P. and Triay, M. "French RSE-M and RCC-MR Code Appendixes for Flaw Analysis: Presentation of the Fracture Parameter Calculation - Part I: General Overview", *International Journal of Pressure Vessels and Piping*, Vol. 84, pp. 590-600, 2007.
[9] Sumpter, J. D. G. and Turner, C. E., "Method for Laboratory Determination of J_c," *Cracks and Fracture*, ASTM STP 601, American Society for Testing and Materials, pp 3-18, 1976.
[10] Cravero, S. and Ruggieri, C., "Estimation Procedure of J-Resistance Curves for SE(T) Fracture Specimens Using Unloading Compliance," *Engineering Fracture Mechanics*, Vol. 74, pp. 2735-2757, 2007.
[11] Cravero, S. and Ruggieri, C., "Further Developments in J Evaluation Procedure for Growing Cracks Based on LLD and CMOD Data," *International Journal of Fracture*, Vol. 148, pp. 387-400, 2007.
[12] American Society for Testing and Materials, "Standard Test Method for Measurement of Fracture Toughness", ASTM E1820, 2001.
[13] Kumar, V., German M. D. and Shih, C. F., "An Engineering Approach to Elastic−Plastic Fracture Analysis", EPRI Report NP-1931, Electric Power Research Institute, Palo Alto, CA, 1981.
[14] Shih, C. F. and Hutchinson, J. W., "Fully Plastic Solutions and Large Scale Yielding Estimates for Plane Stress Crack Problems", T*ransactions of ASME Journal of Engineering Materials and Technology - Series H*, Vol. 98, pp. 289-295, 1976.
[15] Dowling, N. E., *Mechanical Behavior of Materials*, 2nd Edition, Prentice Hall, NJ, 1999.
[16] Zahoor, A., "Ductile Fracture Handbook - Volume 2", EPRI Report NP−6301−D, Electric Power Research Institute, Palo Alto, CA, 1989.
[17] Ainsworth, R. A., "The Assessments of Defects in Structures of Strain Hardening Materials," *Engineering Fracture Mechanics*, Vol. 19, pp. 633-642, 1984.
[18] Kanninen, M. F and Popelar, C. H., *Advanced Fracture Mechanis*, Oxford University Press, New york, 1985.
[19] Koppenhoefer, K., Gullerud, A., Ruggieri, C., Dodds, R. and Healy, B., 1994, ''WARP3D: Dynamic Nonlinear Analysis of Solids Using a Preconditioned Conjugate Gradient Software Architecture,'' *Structural Research Series (SRS) 596*. UILU-ENG-94-2017. University of Illinois at Urbana-Champaign. 1994.
[20] Hughes, T. J. ''Generalization of Selective Integration Procedures to Anisotropic and Nonlinear Media,'' *International Journal for Numerical Methods in Engineering*, Vol. 15, pp. 1413−1418, 1980.
[21] Moran, B., and Shih, C.F., ''A General Treatment of Crack Tip Contour Integrals.'' *International Journal of Fracture*, Vol. 35, pp.295-310, 1987.

8. RESPONSIBILITY NOTICE

The authors are the only responsible for the printed material included in this paper.